High Resolution Phase Shifting Interferometer

Michael R. Bayda

NYMA, Inc., Cleveland, OH 44135

Christoph Bartscher

Technical University of Munich, Germany

R. Allen Wilkinson

NASA Lewis Research Center, Cleveland, OH 44135

Gregory A. Zimmerli

NYMA, Inc., Cleveland, OH 44135

May 21, 1997

Abstract

The configuration, operation, and performance details of a high resolution phase shifting Twyman-Green interferometer are presented. The instrument is used for density relaxation experiments of very compressible liquid-vapor critical fluids. A thin phase-retarding Liquid Crystal Cell (LCC) was placed in the reference arm of the interferometer. The LCC provides four cumulative 90 degree phase shifts to produce four images used in computing each phase map. The Carré technique was used to calculate a phase value for each pixel from the four intensity values of each pixel. Four images for one phase map could be acquired in less than two seconds. The phase resolution of the interferometer in a six second period is better than $\lambda/400$. We demonstrate that a long-term phase stability of $\pm\lambda/65$ can be achieved over a 60 hour period, and is limited by the external environment.

Keywords: Phase-shifting interferometry, Twyman-Green interferometer, Liquid Crystal phase shifter, Carré fringe analysis, critical fluids.

1 INTRODUCTION

Phase shifting interferometry is frequently used to improve the sensitivity and spatial resolution of optical phase measurements. This paper presents a precise phase measurement apparatus using phase shifting interferometry and the Carré technique [1], which is chosen for calculating the optical phase. Detailed information about the Carré technique can be found elsewhere [2].

The approach of the phase shifting technique is to modulate the optical path length in either the test or reference leg of the interferometer in a controlled way during data acquisition. Four modulating steps of the optical path length yield four equations with four unknowns, including the optical phase at each camera pixel. The phase shift can be achieved in several different ways; moving a mirror with a piezoelectric transducer (PZT), using the birefringence of a liquid crystal cell (LCC), or tilting a glass plate. We have integrated the phase shifting capability into a compact thermostated Twyman-Green interferometer, to investigate the density relaxation of very compressible liquid-vapor critical fluids [3]. Phase information yields information about changes in the fluid density. In order to quantify the resolution of the phase measurement, short and long term drifts of the phase measurement are discussed.

2 EXPERIMENT

We investigated two similar setups, one using a low voltage PZT and the other a LCC. Both are phase shifting devices with a negligible heat output. The LCC configuration was

favored because of its better phase shifting stability and repeatability.

Figure 1 shows a schematic of the Twyman-Green interferometer, the LCC phase shifting device and the fluid's test cell. Experiments were performed near the liquid-vapor critical temperature, T_c, of sulfur hexafluoride, SF_6, ($T_c = 318.733$ K), therefore requiring precise temperature control. To measure the density relaxation time constants of the fluid, we require long term phase measurement stability over a period of several hours.

The interferometer unit assembly contained the sample cell, beam splitter, LCC, and mirrors inside a 6 cm diameter by 6 cm long aluminum cylinder which was incorporated into a 2-shell thermostat, temperature controlled to within ± 50 μK. A CCD video camera imaged the interference pattern, and a frame grabbing board digitized the video signal with 8-bit gray scale resolution and stored the images into files. The LCC phase shifter was controlled by a 2 KHz square wave signal, amplitude modulated by a D/A board. The programmed dc voltages in the D/A were activated by TTL trigger signals from the frame grabber board. The video sync signal of the CCD camera was used as a timer, controlling the frame grabbing board and synchronizing the phase shifter with image captures.

3 PHASE CALCULATION

3.1 Carré technique

Carré presented a technique of phase calculation which is independent of the amount of phase shift [1]. The phase is shifted symmetrically about zero by a constant angle α, to yield four equations of the intensity pattern derived from the interference of test and

reference beams:

$$I_1 = I_0 \left\{ 1 + \gamma \cos \left[\phi - \frac{3}{2}\alpha \right] \right\} \quad (1)$$

$$I_2 = I_0 \left\{ 1 + \gamma \cos \left[\phi - \frac{1}{2}\alpha \right] \right\} \quad (2)$$

$$I_3 = I_0 \left\{ 1 + \gamma \cos \left[\phi + \frac{1}{2}\alpha \right] \right\} \quad (3)$$

$$I_4 = I_0 \left\{ 1 + \gamma \cos \left[\phi + \frac{3}{2}\alpha \right] \right\} \quad (4)$$

I_1, I_2, I_3,and I_4 are the measured intensities, I_o is the dc beam intensity, γ is the fringe visibility, and ϕ is the wavefront phase of interest. All of these quantities are functions of pixel location (x, y). Hence, with Eqs.(1-4) ϕ can be calculated independently at each pixel (x, y) of the CCD array and is given by

$$\phi(x, y) = \tan^{-1} \left\{ \frac{\sqrt{|[(I_1 - I_4) + (I_2 - I_3)]\,[3\,(I_2 - I_3) - (I_1 - I_4)]|}}{|(I_2 + I_3) - (I_1 + I_4)|} \right\} \quad (5)$$

with all ϕ in the first quadrant (0 to $\pi/2$). The phase shift α can also be calculated using

$$\alpha(x, y) = 2 \tan^{-1} \left[\sqrt{\frac{3\,(I_2 - I_3) - (I_1 - I_4)}{(I_2 - I_3) + (I_1 - I_4)}} \right] \quad (6)$$

Although a specific phase shift α is not required for this technique, α is usually chosen to be 90° for best resolution [2], hence the fringes are shifted in four steps by −135°, −45°, +45°, and +135°.

To obtain these four cumulative phase shifts of 90°, four specific voltages applied to the LCC phase shifter had to be determined from the calibration curve. We used fringe tracing software to measure the phase shifts during the calibration of the LCC. Equation (6) allows us to verify that the phase shift α is close to the intended value.

3.2 Phase unwrapping

Because of the nature of the arctangent calculations, the equations presented for phase calculation are sufficient only for a modulo $\pi/2$ calculation (Eq. 5). To determine the phase modulo 2π , the signs of quantities proportional to $sin\phi$ and $cos\phi$ must be examined [2, 4].

The removal of modulo 2π phase ambiguities is generally called phase unwrapping, also known as integrating the phase, and can be achieved by comparing the phase difference between adjacent pixels. Information about phase unwrapping, removing noisy or saturated data points, handling bad pixels from anomalies in the visibility γ, filtering, and suggested data processing for those points can be found in various publications [2, 4] and were applied in our algorithms.

Figure 2a shows an interferogram image from a critical fluids experiment at T_c + 9.6 mK, which was phase shifted according to equations (1-4). The phase map shown in figure 2b was obtained after subtracting the background mirror tilt. Note the large phase gradient in the center of the image, which represents a large density variation in the critical region due to the high compressibility of the fluid and earth's gravity. Both x and y-axes represent the pixel position, the z-axis represent the phase in radians including an arbitrary offset.

4 ERROR ANALYSIS

In order to determine the resolution of the phase-shifting interferometer, the fluid's influence on the measured phase was minimized by raising the temperature to $T_c + 2$ K and

allowing enough time for density relaxation before the measurements. Thus, the fluid was in the one-phase state with a nearly uniform index of refraction and controlled to within ± 50 μK. Short and long term tests were performed and the measured phase maps were compared in the time domain. A square image area of 326x326 pixels, covering most of the interferogram of figure 2a, was used for the analysis. A pixel was equivalent to 25x25 μm^2 at the object plane.

4.1 Short-term phase resolution

Sixteen interferogram images were captured in less than six seconds, yielding four phase maps acquired at 1.5 second intervals. Figure 3 illustrates the error distribution of all pixels (326x326x4) of these four phase maps about their mean value. The standard deviation of the distribution is $\lambda/700$. Note the highest occurrences around zero error and the symmetry of the distribution, indicating no systematic errors within the six second interval. This sequence was repeated more than 200 times, consistently leading to similar random error distributions, with standard deviations ranging from $\lambda/730$ to $\lambda/640$.

The error distribution of two phase maps was also calculated. By subtracting one phase map from another, the error distribution of all pixels (326x326) was also random and symmetric about zero error. However the rms deviation ranged from $\lambda/400$ to $\lambda/450$, a value which is consistent with the lower number of samples.

The intensity noise introduced by the 8-bit A/D on the video digitizer board and noise introduced by the CCD camera were the main contributors to the short term error. Vibration and air turbulence were also noticeable short term error factors.

4.2 Long-term phase resolution

The same four phase map sequence described above was repeated at 1 hour intervals over a 60 hour period. The average of each set of four phase maps taken at a given hour was used for the error calculation. The phase map at hour 0 was taken as the reference, and the other 59 phase maps were subtracted from that reference. Figure 4a shows the mean phase error and rms deviation as a function of time. Figure 4b is a plot of room temperature measured during the same period of time. There is a strong correlation of the error with ambient temperature. Thus, the performance is limited by the external influences of the laboratory environment. Nevertheless, we have achieved a phase stability of $\pm\lambda/65$ during the 60 hour period.

Several long-term drift tests were performed, all of which were consistently dependent on room temperature fluctuations. We have observed a maximum phase error of $\lambda/10$ over a 60 hour period, during which the ambient temperature changed by 2 K.

4.3 Setup Optimization

In order to optimize the phase measurements, several aspects concerning the interferometer design need to be considered. Since our measurement resolution was better than $\lambda/400$, all factors had to be investigated.

Air turbulence and vibrations are dynamic variables which reduce the phase measurement precision. A vibration-isolation table supported the experiment to limit vibrations in the fluid and in the mechanical structures. The laser beam paths in the Twyman-Green interferometer were protected from air flows by integration of the interferometer into a

compact thermostat (Figure 1). The paths between the laser and the window of the outer shell of the thermostat, and between the thermostat and the camera were relatively unprotected from air movements induced by the air conditioning of the laboratory. However, a simple plastic cover enclosing the thermostat, laser, and camera eliminated most of the disturbances. Both legs of the interferometer were designed to have equal path lengths in air, to avoid potential barometric pressure effects.

The intensity of the incident laser beam was adjusted to maximize the usable dynamic range of the video digitizer. In addition, a nearly uniform intensity distribution was achieved over the cross section of the incident laser beam. To minimize spurious reflections, most surfaces were anodized black and all optical windows had antireflection coatings.

The effect of room temperature changes on the electronics was also minimized. We monitored the ac signal applied to the LCC phase shifter and found it to be dependent on ambient temperature. A function generator with minimum long term voltage drift was selected, contributing less than $\lambda/400$ drift.

Beam pointing drifts were induced by the steel optical bench top warping slightly with changes in temperature. This kind of optical misalignment also caused the measured intensity to change in magnitude, which was clearly correlated with room temperature. Future work will focus on identifying the components which are most susceptible to changes in the ambient temperature, and minimizing the resulting effects.

5 CONCLUSION

Phase-shifting interferometry is not only a simple and fast process, but also has a precision that is more than ten times better than simply recording interferograms and digitizing the position of fringe maxima or minima. The sensitivity of the phase-shifting technique and our short term resolution of $\lambda/400$ allowed the detection of small phase drifts. One of the challenging tasks in interferometry is the long term stability and repeatability of the results. We have demonstrated that it is possible to achieve a stability in the phase measurement of $\pm\lambda/65$ over a 60 hour period.

In our experiment, the main contributor to the long term phase drifts was the ambient temperature fluctuations in the laboratory. Certainly, enclosing all system components in a temperature controlled environment would be very desirable. Our measurements suggest that a long-term stability of $\pm\lambda/400$ could be achieved in a controlled environment.

6 ACKNOWLEDGMENTS

This work was supported by the Microgravity Fluid Physics branch at NASA Lewis Research Center in Cleveland, Ohio. The authors would like to thank G. Fiedler, K.Y. Min and R. Kusner for their contribution and B. Ovryn for many fruitful discussions.

7 REFERENCES

[1] P. Carré, Installation et utilisation du compateur photoelectrique et interferential du Bureau International des Poids et Mesures, Metrologia 2, 13 (1966).

[2] D. Robinson and G. Reid (ed.'s), Interferogram Analysis: Digital Fringe Pattern Measurement Techniques, Institute of Physics Publishing (1993).

[3] R.A. Wilkinson, Density Relaxation of Liquid-Vapor Critical Fluids in Earth's Gravity (NIST 13th Symposium on Thermophysical Properties (1997).

[4] K. Creath, Phase-shifting speckle interferometry, Applied Optics, Vol. 24, No. 18, p. 3053 (1985).

8 FIGURES

1. Schematic of the Twyman-Green interferometer setup with the Liquid Crystal Cell phase shifter and the fluid test cell.

2. a) An interferogram image at $T_c + 9.6$ mK. b) Phase map of fluid at $T_c + 9.6$ mK after correcting for the mirror tilt.

3. Short term phase error distribution calculated from the average of four phase maps, showing a standard deviation of $\lambda/700$.

4. a) Long term drift of the phase error, and its correlation with b) ambient temperature.

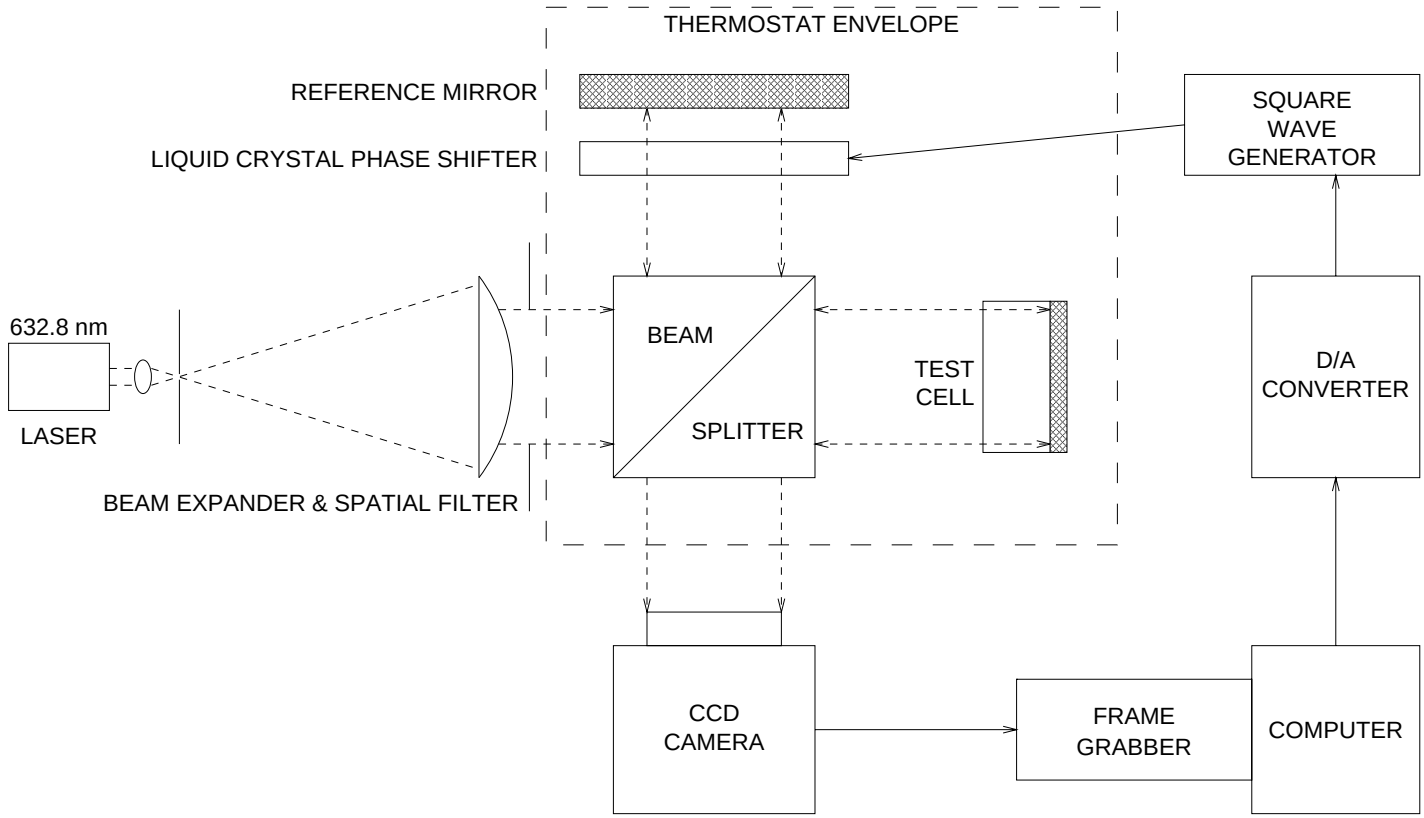

TWYMAN-GREEN PHASE-SHIFTING INTERFEROMETER SCHEMATIC

Figure 1

a)

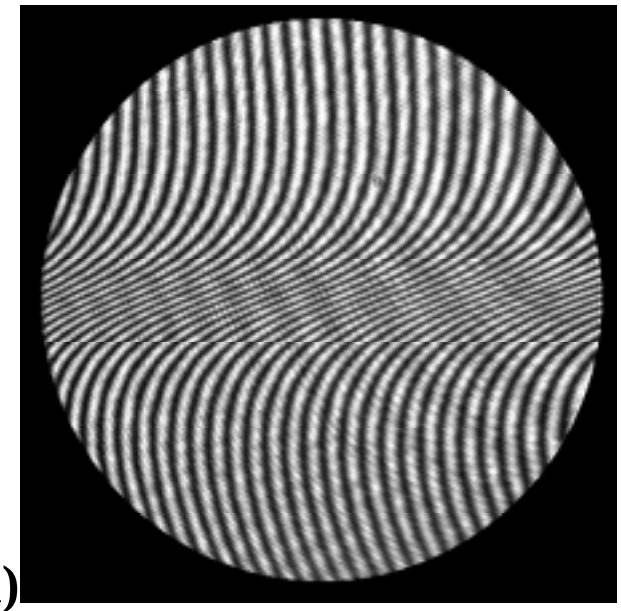

b)

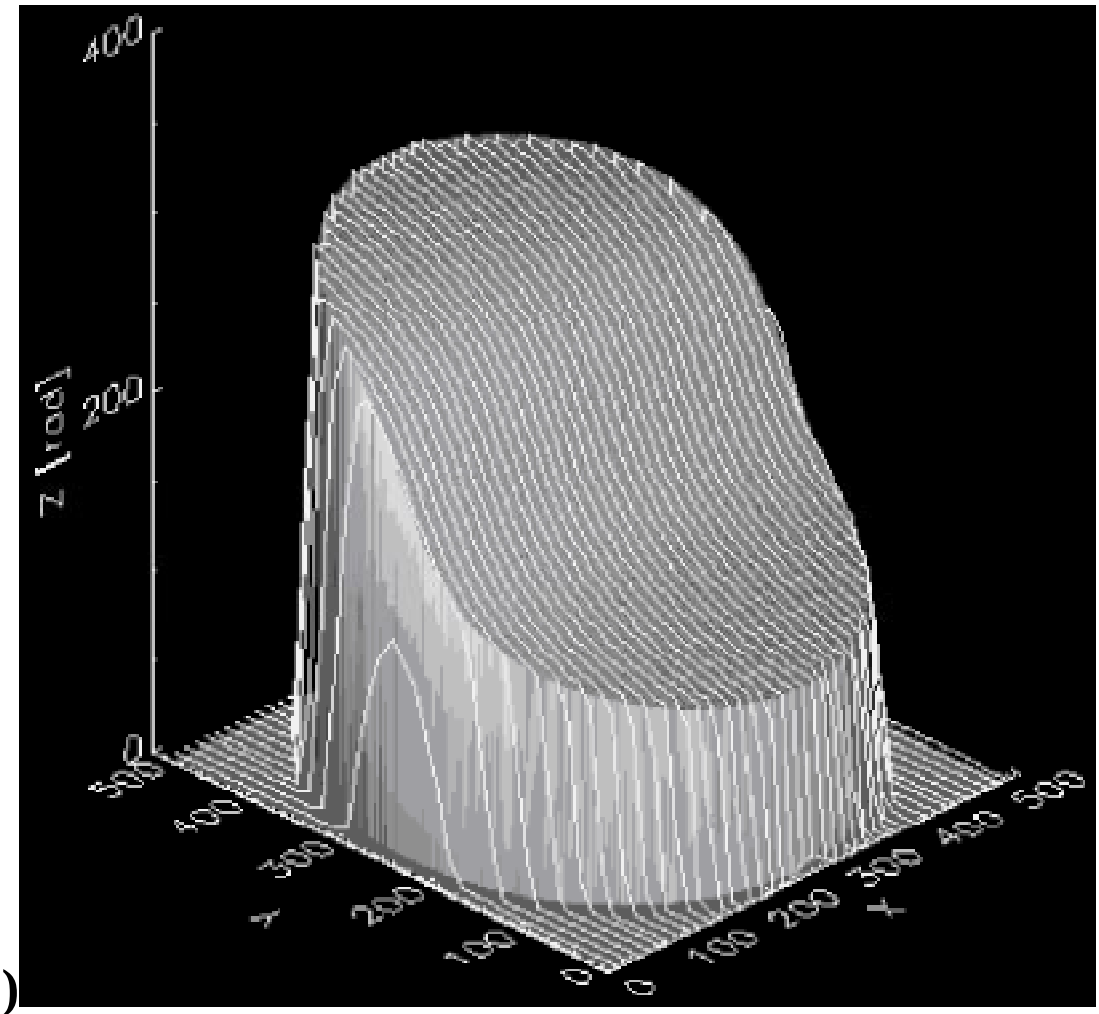

Figure 2

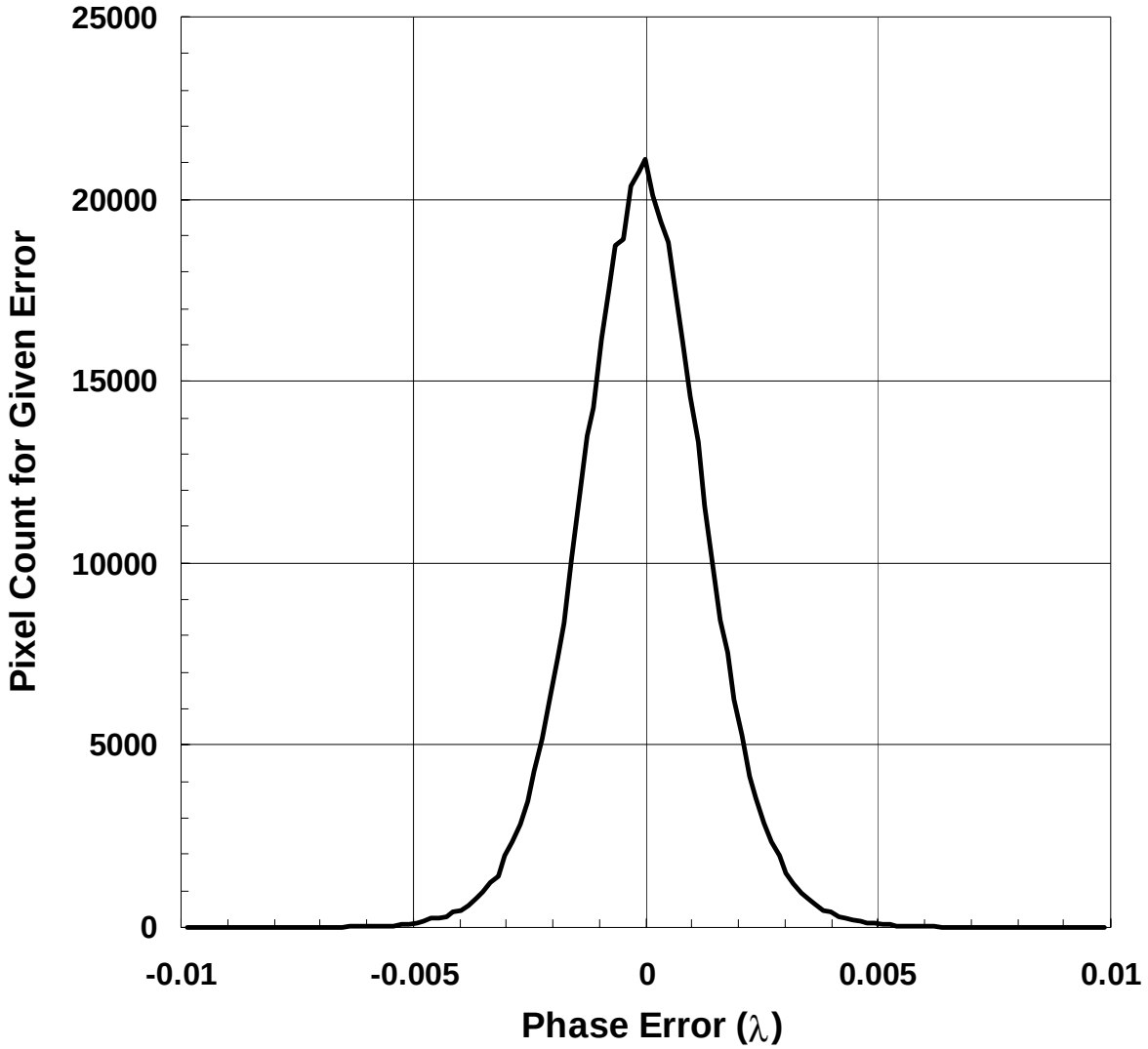
25000
20000
15000
10000
5000
0
Pixel Count for Given Error
-0.01
-0.005
0
0.005
0.01
Phase Error (λ)

Figure 3

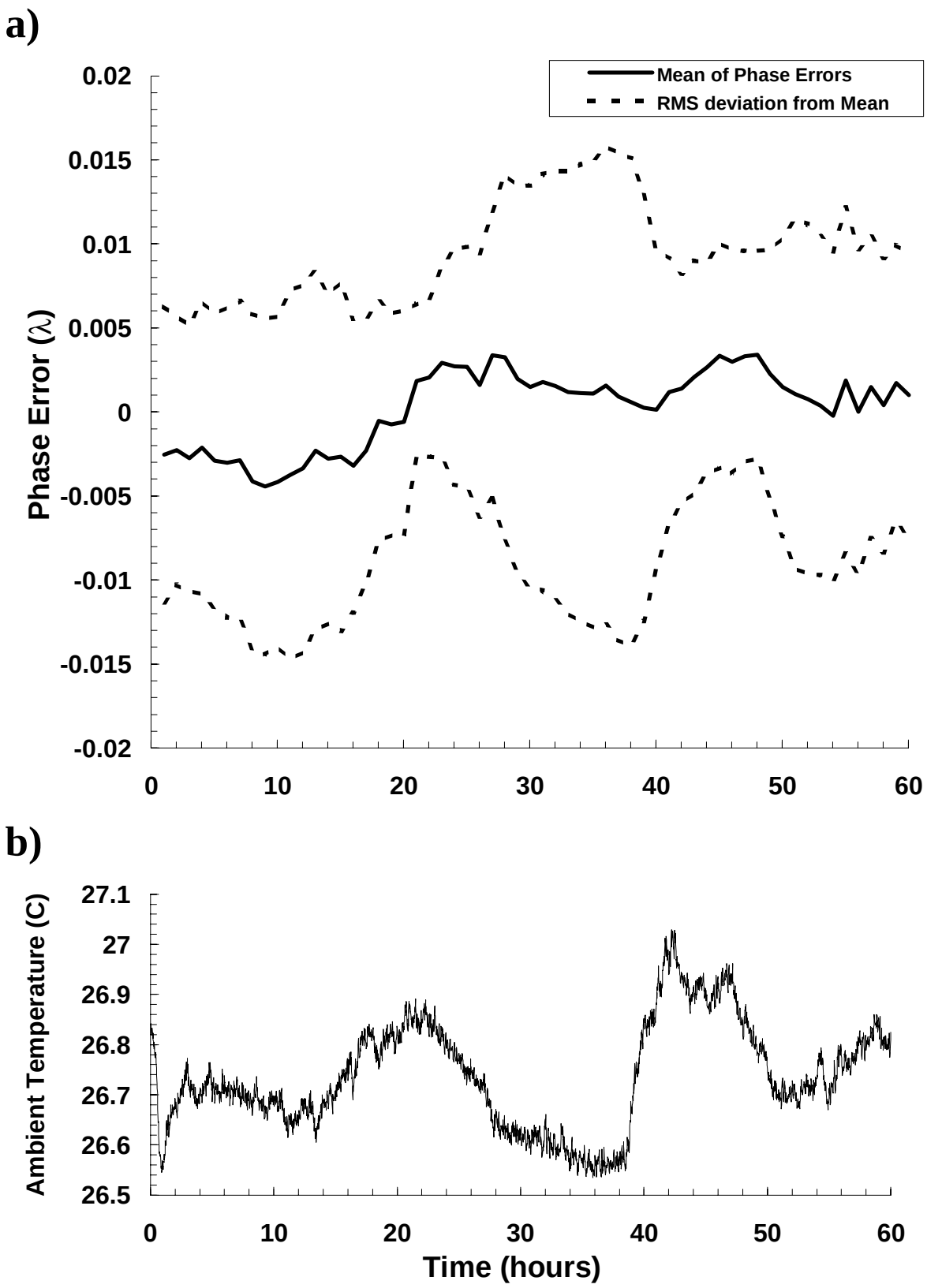
a)
Mean of Phase Errors
RMS deviation from Mean
Phase Error (λ)
0.02
0.015
0.01
0.005
0
-0.005
-0.01
-0.015
-0.02
0
10
20
30
40
50
60
b)
Ambient Temperature (C)
27.1
27
26.9
26.8
26.7
26.6
26.5
0
10
20
30
40
50
60
Time (hours)

Figure 4